Electron removal spectral function of a polaron coupled to dispersive optical phonons

J. Bonča[1,2,*] and S. A. Trugman[3]
[1]*J. Stefan Institute, 1000 Ljubljana, Slovenia*
[2]*Faculty of Mathematics and Physics, University of Ljubljana, 1000 Ljubljana, Slovenia*
[3]*Theoretical Division, Los Alamos National Laboratory (LANL), Los Alamos, New Mexico 87545, USA*

(Received 11 July 2022; revised 6 October 2022; accepted 9 November 2022; published 17 November 2022)

We explore the ground state and thermodynamic properties of the polaron coupled to quantum dispersive optical phonons in one spatial dimension. Calculations are performed using the finite–temperature Lanczos method augmented by a highly efficient construction of the variational Hilbert space. We focus on the electron removal spectral function as relevant for the angle-resolved photoemission experiments. We show that photoemission spectroscopy can be used to measure the phonon dispersion relation in a dilute system of polarons. The spectral weight of observed phonon bands is proportional to the phonon contribution to the wavefunction at finite phonon momentum. In addition, we demonstrate that when removing an electron from a polaron ground state, the polaron band does not appear in the spectral function. The latter becomes observable only at elevated temperatures.

DOI: 10.1103/PhysRevB.106.174303

I. INTRODUCTION

Electron-phonon interaction represents one of the most studied phenomena in solid-state physics. The Holstein model (HM) [1] symbolizes one of the simplest, and possibly the most studied, prototype microscopic models describing electron coupling to quantum lattice degrees of freedom. Despite its apparent simplicity, the model has no exact solution, even in the most straightforward single-electron case. For this reason, many numerical methods have been applied and developed to tackle the ground state and dynamic properties of the HM. The most straightforward are exact diagonalization approaches on finite lattices [2–8] followed by slightly more sophisticated variational approaches [9–22].

Other techniques rely on diagrammatic approaches [23–25] with extensions to momentum-averaged approximations [26–30] that allow for the computation of static as well as dynamic properties of the model. The recently developed hierarchical equations of motion approach allows for computation of spectral functions at finite temperature [31,32]. Further improvements within the context of momentum-averaged approximations led to the development of the generalized Green's function cluster expansion [33] that allows reliable computations in the extreme adiabatic limit of different charge-boson coupled models.

Other successful methods include various Monte Carlo methods [34–40]. The diagrammatic and world line Monte Carlo methods [25,41,42] have recently been applied to determine the mobility of an electron subject to local lattice vibrations. In this class of approaches, density-matrix renormalization-group techniques [43–45] represent yet another class of advanced techniques most successful in tackling the HM in one spatial dimension, which can be easily extended to the finite electron doping regime. Recently, this approach has been generalized to obtain spectral properties of the HM at finite temperatures [46]. In the limit of infinite dimensions, dynamical mean-field theory (DMFT) approaches [47,48] provide exact results, while it has recently been shown that DMFT can also provide a reasonably accurate solution for the spectral function for the one-dimensional (1D) problem [32].

In comparison with multitudes of past research based on the HM, only a few recent works incorporate a more realistic phonon dispersion among the optical Einstein modes. One of the early approaches to include the phonon dispersion in the adiabatic limit has been reported in Ref. [49]. In Ref. [50], authors have investigated the influence of the dispersion among optical phonons on the polaron effective mass. Recently, the electron-addition spectral function and the optical response have been studied in the HM with dispersive optical phonons [51]. The coupling of the electron to acoustic phonons seems to be the most challenging when using various numerical approaches. In such cases, perturbative approaches seem to be more applicable [52,53].

Authors of most previous works on the polaron spectral function have investigated cases of adding an electron (or hole) to the vacuum [5,7,17,26–29,46,51,52,54]. We are in contrast removing an electron from the 1 electron sector. Note that, after the removal of an electron from the system of dispersionless Einstein phonons, there is no dynamics left in the system; the phonon degrees of freedom remain frozen. This is possibly why not much attention has been devoted to the electron removal spectral function in the context of the Holstein polaron. The introduction of dispersion renders the HM more physically relevant, allowing phonon degrees of freedom to evolve even in the absence of the electron. Here, we note that, in most materials, the bandwidth of optical phonons is much smaller than the position of the middle of the optical band. Nevertheless, a substantial dispersion of optical

*janez.bonca@ijs.si

phonons appears in systems where intracellular interactions are comparable with those between cells and where the masses of atoms in the unit cell are similar. A few examples of systems with large dispersions of optical phonons are GaLaAs superlattice systems [55] and hexagonal nitride AlN semiconductors [56].

Our calculation is limited to computation of a single electron coupled to dispersive optical phonons on a 1D chain [57]. Our findings are thus relevant to systems in the low-carrier doping limit with nondegenerate polarons. Recently, angle-resolved photoemission spectroscopy (ARPES) studies have been applied to systems with low electron density, such as doped transition metal oxides [58,59], graphene heterostructures [60], multilayer FeSe thin films [61], and oxide heterostructures [62], where polaronic effects have been observed.

In this paper, we explore the physical properties of the polaron in two directions. We introduce phonon dispersion among optical phonons and examine the electron removal spectral function as relevant for angle-resolved photoemission experiments. We show that photoemission spectroscopy can be used to measure the phonon bands in a dilute system of polarons. In addition, we demonstrate that, when removing an electron from a polaron ground state, the polaron band does not appear in the spectral function. The latter is observed only at elevated temperatures.

II. MODEL AND METHOD

We study a single electron coupled to dispersive optical phonons on a 1D system:

$$H = -t_{\rm el}\sum_j (c_j^\dagger c_{j+1} + {\rm H.c.}) + g\sum_j \hat{n}_j(a_j^\dagger + a_j) + t_{\rm ph}\sum_j (a_j^\dagger a_{j+1} + {\rm H.c.}) + \omega_0 \sum_j a_j^\dagger a_j, \quad (1)$$

where $c_j^\dagger$ and $a_j^\dagger$ are electron and phonon creation operators at site j, respectively, $\hat{n}_j = c_j^\dagger c_j$ represents the electron density operator and $t_{\rm el}$ the nearest-neighbor hopping amplitude. Here, ω_0 denotes the position of the center of the dispersive optical phonon band $\omega(q) = \omega_0 + 2t_{\rm ph}\cos(q)$. We introduce the dimensionless effective electron-phonon coupling strength $\lambda = \epsilon_{\rm p}/2t_{\rm el} = g^2/2t_{\rm el}\sqrt{\omega_0^2 - 4t_{\rm ph}^2}$, where $\epsilon_{\rm p}$ is the polaron energy in the limit $t_{\rm el} = 0$ [50]. From here on, we set $t_{\rm el} = 1$.

We have used the numerical method described in detail in Refs. [12,13,51]. The method generates the variational Hilbert space starting from the initial single-electron Bloch state $c_k^\dagger|\emptyset\rangle$, where $c_k^\dagger = \frac{1}{\sqrt{L}}\sum_j \exp(ikj)c_j^\dagger$, with no phonons on a finite lattice with L sites and periodic boundary conditions. The variational Hilbert space is then generated by applying the first two off-diagonal terms of the Hamiltonian in Eq. (1) N_h times considering the full translational symmetry. In the intermediate coupling regime, the method provides computation of the ground state energy in the thermodynamic limit to extremely high accuracy. The constructed variational Hilbert space allows only a finite maximal distance of phonon quanta from the electron position $L_{\rm max} = N_{\rm h} - 1$. This limitation is in turn responsible for a discrete phonon dispersion $\omega(q)$. Note that $L_{\rm max}$ can be chosen to be smaller than, equal to, or larger than L. Furthermore, the maximal amount of phonon quanta at the electron position is given by $N_{\rm phmax} = N_{\rm h}$, while on the Mth neighboring site to the electron, it is reduced to $N_{\rm phmax} = N_{\rm h} - M$. We have used a standard Lanczos procedure [63] to obtain static as well as dynamic properties of the model.

III. ZERO TEMPERATURE RESULTS

Our main focus is on the electron removal spectral function defined as

$$A(\omega, q) = \sum_{n=0}^{M_0} \left|\langle \psi_{-q}^{(n,0)}|c_q|\psi_0^{(0,1)}\rangle\right|^2 \times \delta\left[\omega - E_q^{(n,0)} + E_0^{(0,1)}\right], \quad (2)$$

where $|\psi_q^{(n,N_{\rm el})}\rangle$ represents the nth translationally invariant state with $N_{\rm el} = 0, 1$ electrons and wave vector q. Specifically, $|\psi_{k=0}^{(0,1)}\rangle$ represents the polaron ground state obtained using the Lanczos procedure. Typically, $M_1 = 50$ Lanczos steps was sufficient to obtain accurate ground state energies and wave functions for the polaron case. Furthermore, we have computed $M_0 = 200$ excited states $|\psi_q^{(n,0)}\rangle$ for each q. To ensure orthogonality of $|\psi_q^{(n,0)}\rangle$, we have also employed the Gram-Schmid reorthogonalization procedure. We have used a Lorentzian form of the delta functions with the half width at half maximum η for graphic representations of $A(q, \omega)$. The integral over ω yields the sum rule:

$$\int_{-\infty}^{+\infty} d\omega A(\omega, q) = \langle \psi_0^{(0,1)}|c_q^\dagger c_q|\psi_0^{(0,1)}\rangle = \bar{n}_q, \quad (3)$$

which further gives $\sum_q \bar{n}_q = 1$ for the case of the polaron. Furthermore, $\bar{n}_q$ contains the information of the expectation value of the kinetic energy via

$$-2t_{\rm el}\sum_q \bar{n}_q \cos(q) = E_{\rm kin}, \quad (4)$$

where $E_{\rm kin} = \langle\psi_0^{(0,1)}|H_{\rm kin}|\psi_0^{(0,1)}\rangle$, and $H_{\rm kin}$ represents the first term in Eq. (1). Equation (4) can serve as a consistency check on the computation of $A(\omega, q)$.

In Fig. 1, we present $\bar{n}_q$ computed in the polaron ground state $|\psi_{q=0}^{(0,1)}\rangle$. In the case of the free electron, i.e., at $\lambda = 0$, $\bar{n}_q = \delta_{q,0}$. Increasing values of $\bar{n}_{q\neq 0}$ at $\lambda > 0$ indicate that the electron obtains finite momenta $q_{\rm el}$ as the phonon cloud picks up the difference $q_{\rm ph}$ so that the total $q = q_{\rm el} + q_{\rm ph} = 0$. In the limit of very large λ (not shown), one expects $\bar{n}_q \sim 1/L$ that would yield, according to Eq. (4), $E_{\rm kin} \to 0$. In the vicinity of $q \sim 0$, a negative value of $t_{\rm ph}$ has a more pronounced effect on the increase of $\bar{n}_q$ than $t_{\rm ph} > 0$. For $t_{\rm ph} = -0.2$, n_q has the largest amplitude of the curves for small q and the smallest amplitude for large q, as one would expect from the energy denominator in the perturbation theory. This effect is more pronounced in the weak coupling regime $\lambda \lesssim 1$, see Fig. 1(a).

In Fig. 2(a), we display $E_{\rm kin}$ vs λ for different values of phonon dispersion. In contrast to $\bar{n}_q$, there is very little effect of different values of $t_{\rm ph}$ on $E_{\rm kin}$ in the weak to intermediate coupling regime, i.e., $\lambda \lesssim 1$. For larger $\lambda > 1$, $t_{\rm ph} > 0$ has a more pronounced effect on $E_{\rm kin}$ than for $t_{\rm ph} < 0$. It is the amplitude of states with large electron momentum q that cause the biggest change in $E_{\rm kin}$. In the first order of the perturbation

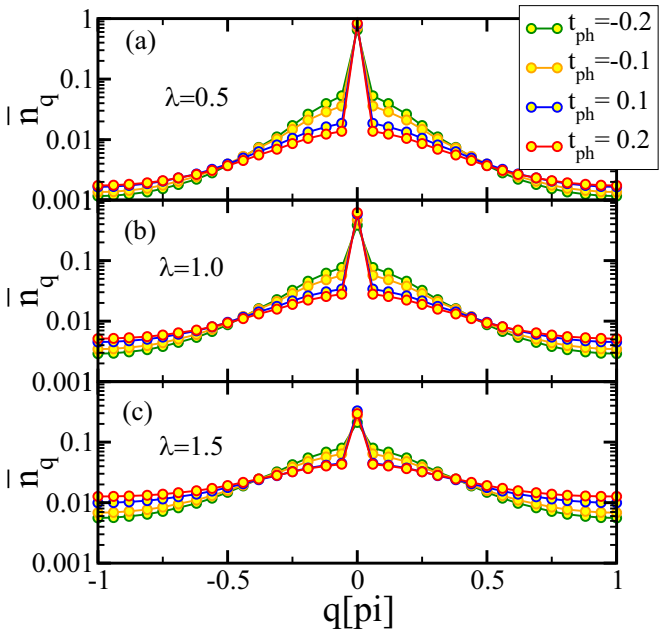

FIG. 1. $\bar{n}_q$ for different values of λ as denoted in insets and for different values of the phonon dispersion $t_{\rm ph}$, computed in the polaron ground state. In this and in all subsequent figures, unless otherwise specified, we have used $\omega_0 = t_{\rm el} = 1$, $N_{\rm h} = 16$, and the size of the system $L = 32$.

theory, the large momentum states have a bigger amplitude for $t_{\rm ph} > 0$ than in the opposite case because the energy denominators are smaller when $t_{\rm ph} > 0$. Note that full lines represent $E_{\rm kin}$ computed as an expectation value of $H_{\rm kin}$ in the polaron ground state, while circles represent $E_{\rm kin}$ obtained from $\bar{n}_q$ via Eqs. (3) and (4).

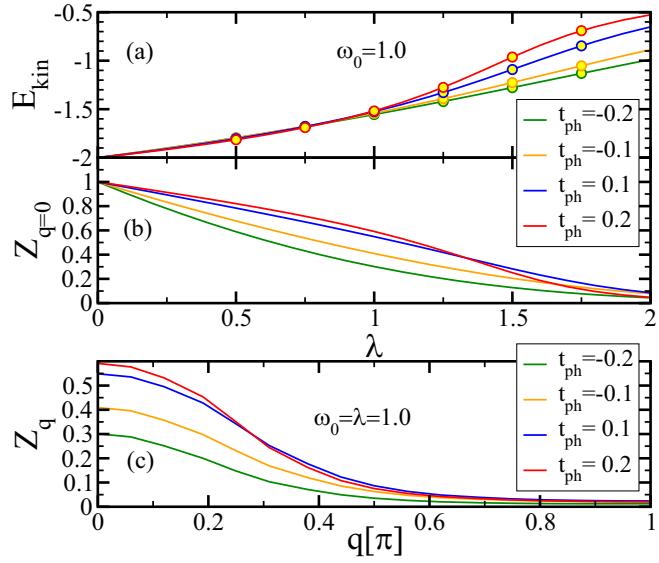

FIG. 2. Full lines in (a) represent $E_{\rm kin}$ of the polaron ground state at various $t_{\rm ph}$ and the total wave vector $q = 0$, open circles represent the same quantity computed using $E_{\rm kin} = -2t_{\rm el}\sum_q \bar{n}_q \cos(q)$. The quasiparticle weight $Z_{q=0}$ vs λ in (b) and (c) represents Z_q at fixed $\lambda = 1$.

Investigating further the effects of $t_{\rm ph}$ on the properties of the polaron, we computed the quasiparticle weight $Z_q = |\langle\psi_q^{(0,1)}|c_q^\dagger|\emptyset\rangle|^2$, which measures the weight of the free electron in the polaron ground state. As shown in Fig. 2(b), $Z_{q=0}$ decreases faster with λ when $t_{\rm ph} < 0$. This is a consequence of the smaller phonon excitation energy $\omega_{q=0} = \omega_0 + 2t_{\rm ph}$ for $t_{\rm ph} < 0$. At large $\lambda \gtrsim 1.5$, we observe a crossing of $Z_{q=0}$ at $t_{\rm ph} = 0.2$ below those computed at smaller values of $t_{\rm ph}$. This seemingly unusual effect can be explained by the coupling of an electron to two phonon excitations, each at $q_1 = q_2 = \pi$, which yields total momentum $q = 0$ and total excitation energy $\omega_{2\rm ph} = 2\omega_0 - 4t_{\rm ph}$. The latter, providing that $t_{\rm ph} > \omega_0/6$, lies below the single-phonon excitation energy at $q = 0$, $\omega_{1\rm ph} = \omega_0 + 2t_{\rm ph}$, see also Ref. [51]. A monotonic decrease of Z_q vs q at fixed $\lambda = 1$ is shown in Fig. 2(c), which indicates diminishing weight of the free electron wave function at given q in the polaron ground state as q departs from the middle of the Brillouin zone (BZ).

We now turn to the analysis of $A(\omega, q)$, presented as density plots for different values of λ and two different values of $t_{\rm ph}$ in Fig. 3. The lowest frequency peaks (lowest $|\omega|$) at $q = 0$ are at the polaron energy $\omega = -E_0^{(0,1)}$. They are represented by the broadened delta functions in the ω and q directions. It is important to emphasize that there is no signature of a polaron band, which is typically observed in the electron-addition spectral function [25–29,31,46,51,52,54]. The reason is that, as the electron is ejected from the polaron ground state, the system has no information about the polaron state at finite momentum. The well-defined dispersive bands seen just below the single polaron peak in all cases represent the single-phonon dispersion given by $\omega_{1\rm ph}(q) = -E_0^{(0,1)} + \omega_0 + 2t_{\rm ph}\cos(q)$, shown in Figs. 3(a)–3(f) as blue dashed lines. While their positions are given by the phonon dispersion relation $\omega_{1\rm ph}(q)$, their spectral weights are nonuniform and largest around $q = 0$, irrespective of the sign of $t_{\rm ph}$. This finding is particularly relevant. By measuring the abovementioned spectral weight of phonon bands, one can extract the weight of the phonon contribution to the wave function at finite phonon momentum q, or more quantitatively, in the weak-coupling regime, the polaron wave function at total $k = 0$ can be written as $|\psi_{k=0}^{(0,1)}\rangle \sim c_{k=0}^\dagger|\emptyset\rangle + \sum_q v_q c_{-q}^\dagger a_q^\dagger|\emptyset\rangle$. Then the q-dependent intensity of phonon bands is proportional to $|v_q|^2$.

In addition to the single-phonon band, two- and even three-phonon continuums are clearly seen for $\lambda \gtrsim 1.0$. The two-phonon continuum is located in the interval given by $\omega_{2\rm ph}^{\pm} = -E_0^{(0,1)} + 2\omega_0 \pm 4t_{\rm ph}\cos(q/2)$, as indicated by the yellow dot-dashed lines. The three-phonon one appears between $\omega_{3\rm ph}^{-} = -E_0^{(0,1)} + 3\omega_0 - 4t_{\rm ph}\cos[(q \pm \pi)/3]$ and $\omega_{3\rm ph}^{+} = -E_0^{(0,1)} + 3\omega_0 + 4t_{\rm ph}\cos(q/3)$ for $t_{\rm ph} > 0$ [indicated by red dashed lines in Figs. 3(e) and 3(f)]. The upper and lower bounds are reversed for $t_{\rm ph} < 0$.

While the polaron dispersion does not appear in the electron removal spectral function $A(\omega, q)$, the dispersion can be detected by removing an electron from a polaron state with a given total momentum k, $\psi_k^{(0,1)}$:

$$A(\omega, q, k) = \sum_n \left|\left\langle\psi_{k-q}^{(n,0)}\middle|c_q\middle|\psi_k^{(0,1)}\right\rangle\right|^2 \times \delta\left[\omega - E_{k-q}^{(n,0)} + E_k^{(0,1)}\right], \quad (5)$$

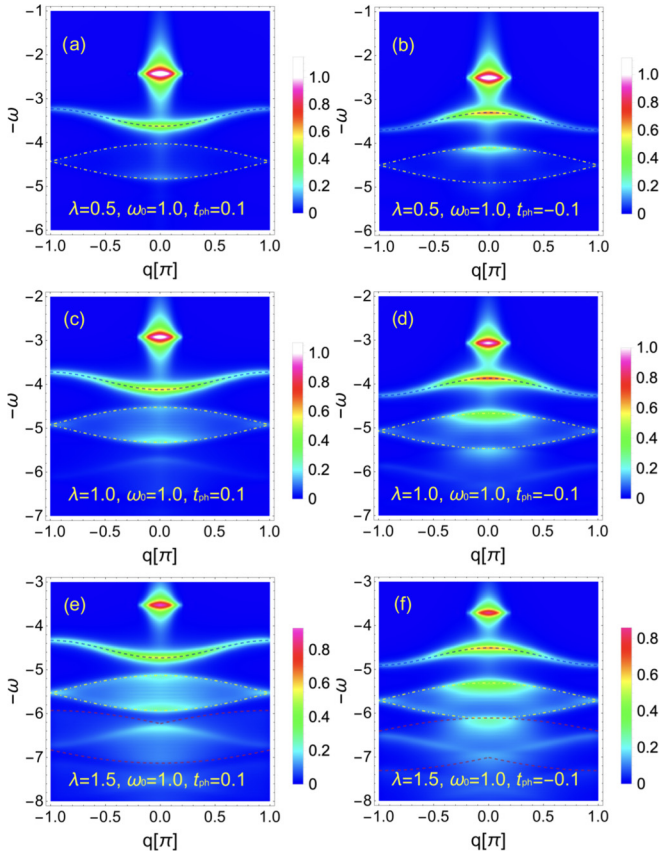

FIG. 3. $A(\omega, q)$ for different λ and $t_{\rm ph}$ as denoted in the insets. In (a)–(f), blue dashed lines follow single-phonon excitation and are obtained from $\omega_{1\rm ph} = -E^{(0,1)}_{q=0} + \omega_0 + 2t_{\rm ph}\cos(q)$, yellow dot-dashed lines enclose the continuum of two-phonon excitations below the polaron ground state energy: $\omega^{\pm}_{2\rm ph} = -E^{(0,1)}_{q=0} + 2\omega_0 \pm 4t_{\rm ph}\cos(q/2)$. In addition, red dashed lines indicate the regime of three-phonon excitation continuum $\omega^{\pm}_{3\rm ph}$, as given in the text. We have used artificial broadening $\eta = 0.05$. Note that the lowest frequency (lowest $|\omega|$) peaks at $q = 0$ are represented by the Lorentzian forms of the delta functions in q and ω. Identical color coding has been used in all panels.

In Fig. 4, we present $A(\omega, q, k)$ for $k > 0$, while in Figs. 3(c) and 3(d), results for the same set of parameters are presented for $k = 0$. With increasing k the lowest $|\omega|$ peak follows the polaron dispersion relation $\omega_{\rm pol}(q) = -E^{(0,1)}_{q}$, as denoted by the white dashed lines, while its spectral weight decreases. This is consistent with the notion that the spectral weight of this peak corresponds to the quasiparticle weight given by $Z_q = |\langle\psi^{(0,1)}_{q}|c^{\dagger}_{q}|\psi^{(0,0)}_{q=0}\rangle|^2$, where the state $|\psi^{(0,0)}_{q=0}\rangle$ represents the electron and phonon vacuum. Also, Z_q is displayed in Fig. 2(c). At higher ω single- and multiple phonon bands shifted by $q \to q - k$ remain clearly visible, while most of their spectral weight remains around $q = 0$. One way to think about this is that, at weak coupling, the polaron ground state at large k is mainly composed of an electron at (near) zero momentum and a phonon of momentum (near) k, when this is the lowest energy state of total momentum k. That is why the spectral weight peaks near $q = 0$. At larger k, we observe a shift of the spectral weight from the polaron peak to phonon bands.

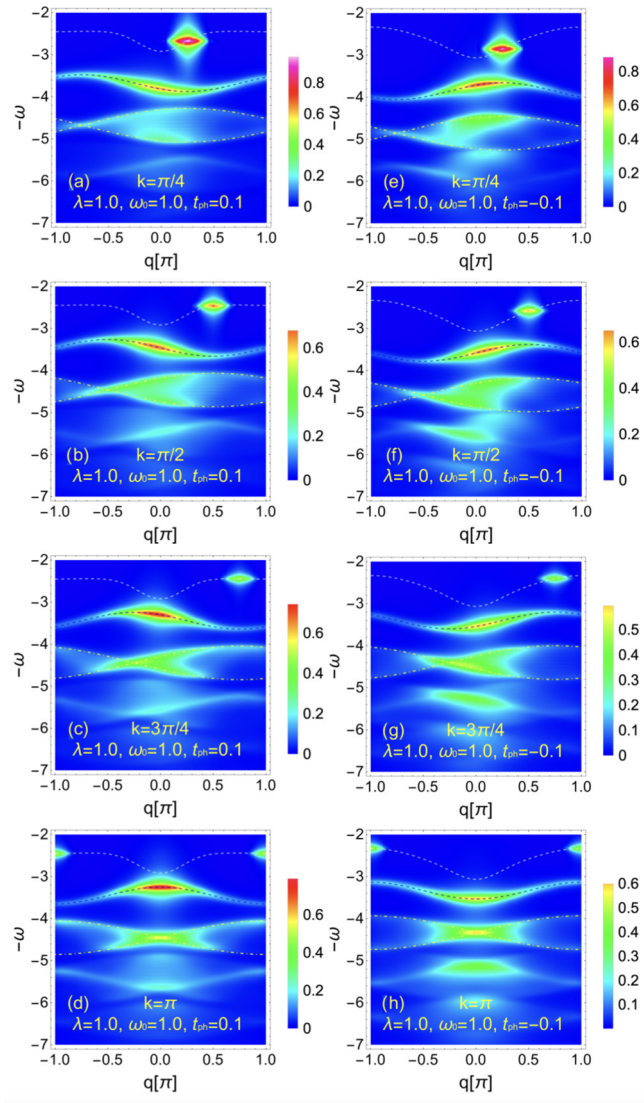

FIG. 4. $A(\omega, q, k)$ computed at (a)–(d) $t_{\rm ph} = 0.1$ and (e)–(h) $t_{\rm ph} = -0.1$, for different values of k as denoted in the insets. In (a)–(e), blue dashed lines follow single-phonon excitation and are obtained from $\omega_{1\rm ph} = -E^{(0,1)}_{k} + \omega_0 + 2t_{\rm ph}\cos(q-k)$, yellow dot-dashed lines enclose the continuum of two-phonon excitations below the polaron ground state energy: $\omega^{\pm}_{2\rm ph} = -E^{(0,1)}_{k} + 2\omega_0 \pm 4t_{\rm ph}\cos[(q-k)/2]$. White dashed lines represent the polaron dispersion relation given by $\omega_{\rm pol} = -E^{(0,1)}_{q}$. We have used artificial broadening $\eta = 0.05$. Note that the lowest frequency (lowest $|\omega|$) peaks at $q = 0$ are represented by the Lorentzian forms of the delta functions in q and ω. Identical color coding has been used in all panels.

IV. THERMODYNAMIC PROPERTIES

Computation of static quantities was done using the finite temperature Lanczos method (FTLM) [54,64]. The central proposition of the method is that the summation over all states in a given sector can be replaced by the summation over normalized random states $|r_k\rangle = \sum_{j=1}^{N_1}\alpha_j|\phi^{(j,1)}_{k}\rangle$, where α_j are distributed randomly from a uniform distribution, and $|\phi^{(j,1)}_{k}\rangle$ represents N_1 translationally invariant basis states in the one-electron and multiphonon subspace. The expectation

value of a given operator B is obtained from

$$\langle B\rangle = \mathcal{Z}^{-1}\sum_{k}\sum_{r=1}^{R}\sum_{m=1}^{M_1}\exp\left[-\beta E_k^{(m,1)}\right]\langle r_k|\psi_k^{(m,1)}\rangle \times\langle\psi_k^{(m,1)}|B|r_k\rangle, \tag{6}$$

where $|\psi_k^{(m,1)}\rangle$ and $E_k^{(m,1)}$ are Lanczos wave functions and corresponding energies in the 1 electron subspace and $\beta = 1/T$. Lanczos states are generated using M_1 iterations starting from $|r_k\rangle$ states, respectively. Furthermore, R represents the number of different random states, and the first summation is over all nonequivalent k states in the first BZ. The statistical sum $\mathcal{Z}$ is in the framework of the FTLM method [54,64] given by

$$\mathcal{Z} = \sum_{k}\sum_{r=1}^{R}\sum_{m=1}^{M_1}\exp\left[-\beta E_k^{(m,1)}\right]\left|\langle r_k|\psi_k^{(m,1)}\rangle\right|^2. \tag{7}$$

For computation of static properties, we have sampled over $R = 200$ random states and performed $M_0 = 100$ Lanczos iterations.

Computation of dynamic properties at finite temperature, such as the electron-removal spectral function $A(\omega, q, T)$, requires additional summation over the zero electron states. Here, $A(\omega, q, T)$ is expressed as

$$\begin{aligned}A(\omega,q,T) = \mathcal{Z}^{-1}\sum_{k}\sum_{r=1}^{R}\sum_{m=1}^{M_1}\sum_{n=1}^{M_0}&\exp\left[-\beta E_k^{(m,1)}\right]\\ &\times\langle r_k|\psi_k^{(m,1)}\rangle\langle\psi_k^{(m,1)}|c_q^\dagger|\psi_{k-q}^{(n,0)}\rangle\\ &\times\langle\psi_{k-q}^{(n,0)}|c_q|r_k\rangle\\ &\times\delta\left[\omega - E_{k-q}^{(n,0)} + E_k^{(m,1)}\right],\end{aligned} \tag{8}$$

where $|\psi_k^{(m,l)}\rangle$ and $E_k^{(m,l)}$ are Lanczos wave functions and corresponding energies in the $l = 0$ and 1 electron subspace. Lanczos states in the $l = 0$ and 1 sectors are generated using M_0 and M_1 iterations starting from $c_q|r_k\rangle$ and $|r_k\rangle$ states, respectively. We have typically used $R = 200$, $M_1 = 50$, and $M_0 = 100$ Lanczos iterations combined with the Gram-Schmidt reorthogonalization procedure to avoid spurious nonorthogonal states that appear due to roundoff errors, introduced by the finite-precision arithmetic when using large values of M_i.

As a consistency check, we note that the frequency sum rule yields

$$\int_{-\infty}^{+\infty} d\omega A(\omega,q,T) = \langle c_q^\dagger c_q\rangle, \tag{9}$$

$$\langle H_{\rm kin}\rangle = -2t_{\rm el}\sum_{q}\langle c_q^\dagger c_q\rangle\cos(q), \tag{10}$$

which in turn also defines the thermodynamic average of the kinetic energy $\langle H_{\rm kin}\rangle$. In Fig. 5(d), we compare results of $\langle H_{\rm kin}\rangle$ computed using Eq. (6) with those obtained from sum rules following Eqs. (9) and (10).

We first discuss selected T-dependent static properties. We separate the Hamiltonian in Eq. (1) into three parts: $H_{\rm kin}$, which represents the first term in Eq. (1), $H_{\rm ep}$ the second, and $H_{\rm ph}$ the sum of the last two terms. In Fig. 5, we show thermodynamic averages of the total energy $\langle H\rangle$ and the three parts of

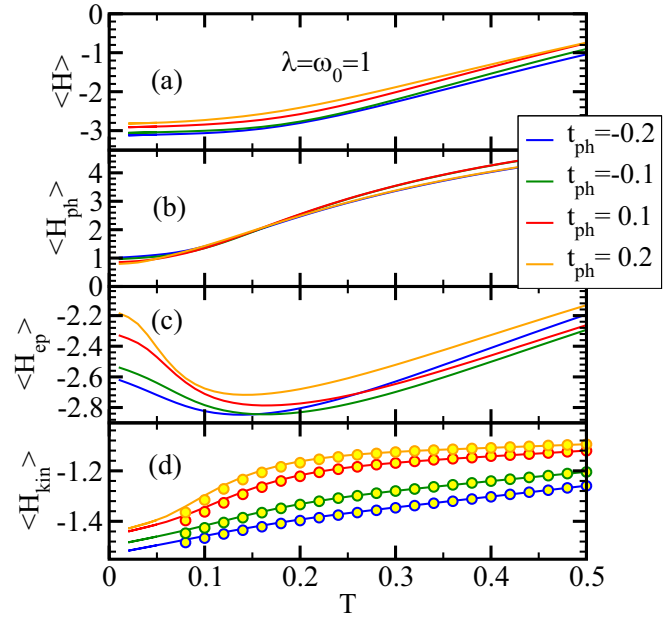

FIG. 5. Temperature dependence of $\langle H\rangle$, $\langle H_{\rm ph}\rangle$, $\langle H_{\rm ep}\rangle$, and $\langle H_{\rm kin}\rangle$ in (a)–(d) for different values of $t_{\rm ph}$, as indicated in the inset. In (d), circles present results obtained from spectral function frequency sum rules using Eqs. (9) and (10).

H for different strengths of the optical dispersion $t_{\rm ph}$. The total energy $\langle H\rangle$ remains nearly T independent for $T \lesssim 0.1\omega_0$, followed by a monotonic increase at higher T. In contrast, we observe a noticeable redistribution of energies between different parts of H even for $T \lesssim 0.1\omega_0$. Here, $\langle H_{\rm kin}\rangle$ and $\langle H_{\rm ph}\rangle$ show pronounced increase with T in the low-T regime. In contrast, $\langle H_{\rm ep}\rangle$ displays a decrease that compensates the increase of the former two, considering the equality $\langle H\rangle = \langle H_{\rm kin}\rangle + \langle H_{\rm ph}\rangle + \langle H_{\rm ep}\rangle$. The lowering of the electron-phonon coupling term $\langle H_{\rm ep}\rangle$ results from the thermal population of polaron states at finite k that possess lower electron-phonon energy and higher kinetic energy. A more detailed analysis is given in the Appendix. Note that, in the high-T limit as $T \to \infty$, $\langle H_{\rm kin}\rangle \to 0$.

We conclude with the analysis of spectral functions at finite T. At small $T = 0.1\omega_0$, we compare $A(\omega, q, T)$ in Figs. 6(a) and 6(e) with their $T = 0$ counterparts in Figs. 3(c) and 3(d). The lowest $|\omega|$ peak represented with a single delta function in ω and q at $T = 0$ obtains finite widths, first along the q axis, then at higher T also along the ω axis. The spread along the q direction is most pronounced along the polaron dispersion relation $\omega_{\rm pol}(q) = -E_q^{(0,1)}$, as marked by white dashed lines, and becomes even more evident at higher T. The spread is due to processes where an electron with finite q is ejected from the thermally excited polaron state $|\psi_k^{(0,1)}\rangle$ at $q = k$. The increased spectral weight in the $\omega > \omega_{\rm pol}(q)$ direction is most evident around $q = 0$. It is a consequence of transitions where an electron with $q = 0$ is ejected from the same thermally excited state of the polaron at finite k as in the previous case.

Next, we analyze the well-defined single-phonon excitation relation $\omega_{\rm 1ph}(q)$. In contrast to the $T = 0$ case, as shown in Figs. 3(c) and 3(d), at finite T, for the same set of parameters presented in Fig. 6, a continuum of

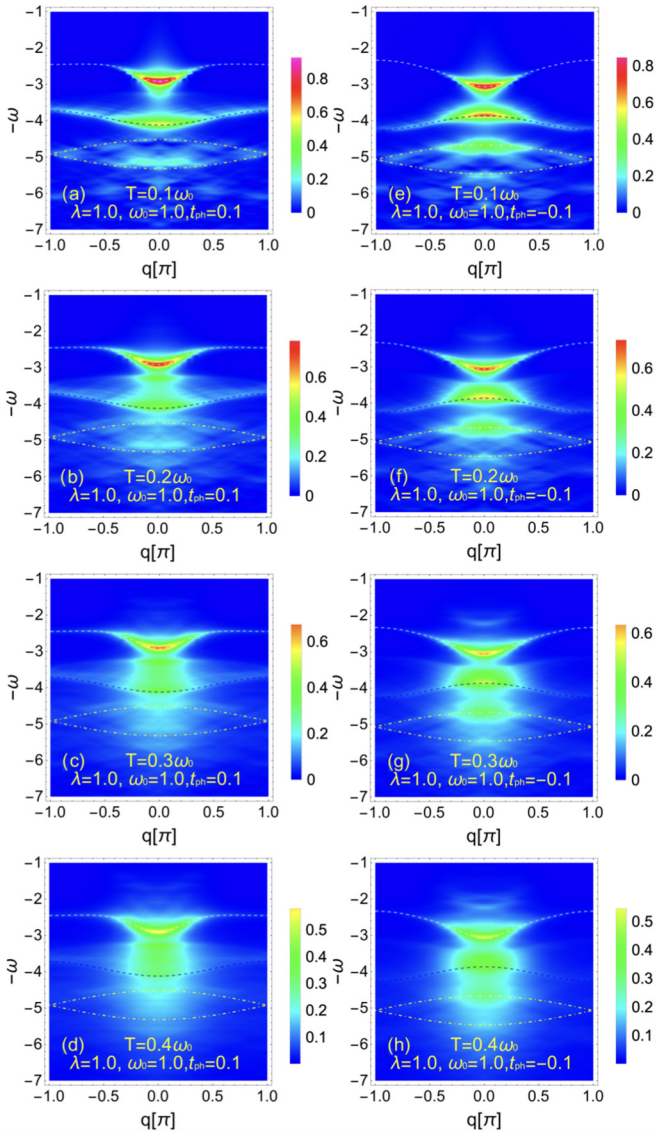

FIG. 6. $A(\omega, q, T)$ computed at (a)–(d) $t_{\rm ph} = 0.1$ and (e)–(h) $t_{\rm ph} = -0.1$, for different values of T, as denoted in the insets. Blue dashed lines follow the single-phonon excitation and are obtained from $\omega_{1\rm ph}(q) = -E^{(0,1)}_{q=0} + \omega_0 + 2t_{\rm ph}\cos(q)$, yellow dot-dashed lines enclose the continuum of two-phonon excitations below the polaron ground state energy: $\omega^{\pm}_{2\rm ph} = -E^{(0,1)}_{q=0} + 2\omega_0 \pm 4t_{\rm ph}\cos[(q)/2]$. White dashed lines represent the polaron dispersion relation given by $\omega_{\rm pol}(q) = -E^{(0,1)}_{q}$. We have used artificial broadening $\eta = 0.05$. Identical color coding has been used in all panels.

excitations appears above the single-phonon excitation band, i.e., at $|\omega| < |\omega_{1\rm ph}(q)|$, while $\omega_{1\rm ph}(q)$ now defines the lower limit of the continuum of single-phonon excitations. The continuum is most clearly observed in the interval $0.2 \lesssim T/\omega_0 \lesssim 0.3$. Additional spectral weight also appears below and above the boundaries of the two-phonon continuum already at $T \gtrsim 0.1\omega_0$. At $T \gtrsim 0.4\omega_0$, the boundaries of single- and multiple phonon excitations become indistinguishable from the background, while additional spectral weight appears around $q = 0$ above $\omega_{\rm pol}(q)$. The latter is a consequence of an electron ejected from an excited polaron state at around $q = 0$ composed of a polaron with an additional phonon excitation to a final state with no (or, more generally, fewer) phonons.

V. CONCLUSIONS

We computed selected static and dynamic properties of the electron coupled to dispersive optical phonons in the framework of the HM at zero and finite temperature. The introduction of phonon dispersion has a nearly undetectable effect on the kinetic energy in the weak to intermediate coupling regime. In contrast, we find a substantial variation of the quasiparticle weight with varying phonon bandwidth already in the weak coupling regime. The upward dispersion ($t_{\rm ph} < 0$) has a more decisive influence on the quasiparticle weight than the downward one.

We have computed the electron-removal spectral function of a polaron coupled to dispersive quantum optical phonons. In contrast to the most commonly computed electron-addition spectral function that yields unity for the frequency sum rule, the sum rule of the electron-removal spectral function from the polaron state is given by the expectation value of the density operator n_q. Moreover, using Eq. (4), n_q yields the expectation value of the kinetic energy operator.

The spectral function computed in the ground polaron state consists of a single peak positioned at the polaron frequency with its weight given by $Z_{q=0}$ and well-defined single- and multiple phonon bands that precisely follow single- and multiple phonon dispersion relations shifted by the polaron energy. Their spectral weight is not uniform but predominantly concentrated near the middle of the BZ.

At finite temperatures, the total energy remains nearly T independent up to $T \lesssim 0.1\omega_0$, followed by a monotononic increase at higher T. In contrast, in the same temperature regime, we observe a noticeable redistribution of energies between different parts of H. While the kinetic and phonon energy show a pronounced increase with T, the electron-phonon coupling energy decreases with increasing T. The latter results from the thermal population of polaron states at finite q that possess lower electron-phonon energy.

The electron-removal spectral function undergoes distinct changes at finite temperatures. The low-frequency peak obtains a finite width and disperses along the direction of the polaron band. Additional spectral weight appears as a satellite peak above the zero-T low-frequency peak in the middle of the BZ. The latter is a consequence of an electron ejected from an excited polaron state composed of a polaron with an additional phonon excitation. Extra spectral weight develops also above the phonon excitation band, which remains distinguishable from the rest of the spectra up to $T \lesssim 0.3\omega_0$. The electron-removal spectral function frequency sum rule is consistent with the prediction of Eq. (10) down to $T \sim 0.1\omega_0$ and serves as a consistency check of the numerical method at finite T.

We have shown that photoemission spectroscopy can be used to measure the phonon dispersion relation in a dilute system of polarons. We have demonstrated that the polaron band does not appear in the spectral function when removing an electron from a polaron ground state. The latter becomes

observable only at elevated temperatures. We have also shown that the spectral weight of observed phonon bands is proportional to the phonon contribution to the wave function at finite phonon momentum q.

We conclude by comparing our results in Figs. 3 and 6 with ARPES measurements [58] in the low-doped transition metal oxide TiO_2, where at least one satellite has been observed below a polaron peak. Both signals are limited to the proximity of the center of the BZ. The separation of the satellite peak from the polaron one corresponds to the longitudinal-optical phonon.

Before comparing our findings with ARPES data, we note that our calculations are based on a single electron. Our results predict that, in the extremely low-doping regime, only a single polaron peak located in the middle of the BZ should be observed at extremely low T. Still, at finite T, even a calculation considering a single electron predicts the observation of a polaron band around the center of the BZ that appears due to thermal excitations of polaron states at the finite center of mass wave vector. Concerning the satellite peak in Ref. [58], our results obtained at $T = 0$ predict the observation of a dispersive phonon band with the largest intensity around the center of the BZ. With increasing T, the phonon band spreads out and loses intensity.

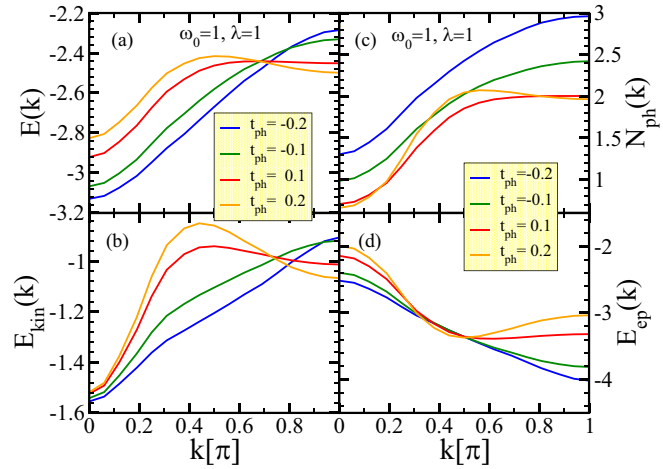

FIG. 7. Zero-T results vs k: (a) the polaron dispersion relation $E(k) = \langle\psi_k^{(0,1)}|H|\psi_k^{(0,1)}\rangle$, (b) the kinetic energy $E_{\rm kin}(k) = \langle\psi_k^{(0,1)}|H_{\rm kin}|\psi_k^{(0,1)}\rangle$, (c) the total number of phonons in the system $N_{\rm ph}(k) = \langle\psi_k^{(0,1)}|\sum_j a_j^\dagger a_j|\psi_k^{(0,1)}\rangle$, and (d) the electron-phonon coupling $E_{\rm ep}(k) = \langle\psi_k^{(0,1)}|g\sum_j n_j(a_j + a_j^\dagger)|\psi_k^{(0,1)}\rangle$.

ACKNOWLEDGMENTS

J.B. acknowledges the support by the Program P1-0044 of the Slovenian Research Agency. J.B. and S.A.T. acknowledge support from the Center for Integrated Nanotechnologies, a U.S. Department of Energy, Office of Basic Energy Sciences user facility. S.A.T. acknowledges support from LANL Laboratory Directed Research and Development.

APPENDIX: WHY DOES $\langle H_{\rm ep}\rangle$ DECREASE WITH T?

1. Numerical argument

We give further insight into the seemingly unexpected initial decrease of the electron-phonon coupling energy with T, as observed in Fig. 5(c). With increasing T, the states with nonzero total momentum k become thermally populated at much lower T than ω_0 since the entire polaron energy band $E(k)$ is narrower than ω_0, see also Fig. 7(a), while states at small k are even much closer to the ground state energy. It is instructive to analyze results obtained at zero T as functions of k. In Fig. 7(d), we show that, with increasing k, the electron-phonon energy $E_{\rm ep}$ decreases as the electron becomes more strongly coupled to the phonon cloud. This trend is also explained using the second-order perturbation theory in Appendix A 2. Consequently, the number of phonons in the system $N_{\rm ph}$ increases. We conclude that the decrease of $\langle H_{\rm ep}\rangle$ is a consequence of the thermal population of states with finite k that are more strongly coupled to the electron.

The thermal population of states with finite k can also explain why the total number of phonons in the systems, approximately given by $N_{\rm ph}(T) = \langle H_{\rm ph}\rangle/\omega_0$, as seen in Fig. 5(b), increases by $N_{\rm ph}(T) - N_{\rm ph}(0) \sim 2$ at relatively small temperatures $T \sim 0.2\omega_0$.

2. Analytical argument

Consider $E(k)$ in leading order perturbation theory for the polaron ground state at total momentum k, for dispersionless optical phonons at weak coupling.

Here, $\Delta E(k)$ in the second order in g is given by

$$\Delta E(k) = \sum_q \frac{|\langle\emptyset|c_{k+q}a_{-q}|H_{\rm ep}c_k^\dagger|\emptyset\rangle|^2}{\epsilon^0(k) - [\epsilon^0(k+q) + \omega_0]}, \qquad \text{(A1)}$$

where $H_{\rm ep}$ is the electron-phonon Hamiltonian in the reciprocal space, $\epsilon^0(k) = -2t\cos(k)$ is the unperturbed electron energy at momentum k, while the energies of the unperturbed excited states with one phonon and one electron lie above $-2t + \omega_0$. As the polaron momentum k increases, $\epsilon_0(k)$ increases, but the set of unperturbed excited states $-2t\cos(k+q) + \omega_0$ are at the same energies as for $k = 0$ since q spans the entire BZ. (Whatever the total momentum, there is always an unperturbed excited state with the electron at zero momentum and the phonon taking the rest of the momentum.) It therefore follows that $\Delta E(k)$ at nonzero k is the same as $\Delta E(k)$ at $k = 0$ but with a reduced phonon energy $\tilde\omega = \omega_0 - [\epsilon^0(k) - \epsilon^0(0)]$. As k increases, the dimensionless coupling $g/\tilde\omega$ increases, and $\Delta E(k)$ becomes larger in magnitude (more negative). Since $\Delta E(k) = \Delta E_{\rm ep}(k) + \Delta E_{\rm kin}(k) + \Delta E_{\rm ph}(k)$, and the last two terms are positive, $\Delta E_{\rm ep}(k) \leqslant \Delta E(k)$.

Thus, as the temperature increases from zero and thermally populates nonzero polaron states, $\langle H_{\rm ep}\rangle$ becomes more negative (in weak coupling).

[1] T. Holstein, Ann. Phys. **8**, 325 (1959).
[2] J. Ranninger and U. Thibblin, Phys. Rev. B **45**, 7730 (1992).
[3] F. Marsiglio, Phys. Lett. A **180**, 280 (1993).
[4] A. S. Alexandrov, V. V. Kabanov, and D. K. Ray, Phys. Rev. B **49**, 9915 (1994).
[5] H. Fehske, J. Loos, and G. Wellein, Z. Phys. B **104**, 619 (1997).
[6] B. Bäuml, G. Wellein, and H. Fehske, Phys. Rev. B **58**, 3663 (1998).
[7] H. Fehske, J. Loos, and G. Wellein, Phys. Rev. B **61**, 8016 (2000).
[8] M. Hohenadler, M. Aichhorn, and W. von der Linden, Phys. Rev. B **68**, 184304 (2003).
[9] G. Wellein and H. Fehske, Phys. Rev. B **56**, 4513 (1997).
[10] A. W. Romero, D. W. Brown, and K. Lindenberg, J. Chem. Phys. **109**, 6540 (1998).
[11] G. Wellein and H. Fehske, Phys. Rev. B **58**, 6208 (1998).
[12] J. Bonča, S. A. Trugman, and I. Batistić, Phys. Rev. B **60**, 1633 (1999).
[13] L.-C. Ku, S. A. Trugman, and J. Bonča, Phys. Rev. B **65**, 174306 (2002).
[14] O. S. Barišić, Phys. Rev. B **65**, 144301 (2002).
[15] O. S. Barišić, Phys. Rev. B **69**, 064302 (2004).
[16] O. S. Barišić, Phys. Rev. B **73**, 214304 (2006).
[17] G. De Filippis, V. Cataudella, V. Marigliano Ramaglia, and C. A. Perroni, Phys. Rev. B **72**, 014307 (2005).
[18] H. Fehske and S. A. Trugman, Numerical solution of the Holstein polaron problem, in *Polarons in Advanced Materials*, edited by A. S. Alexandrov (Springer, Dordrecht, 2007), pp. 393–461.
[19] A. Alvermann, H. Fehske, and S. A. Trugman, Phys. Rev. B **81**, 165113 (2010).
[20] T. Ohgoe and M. Imada, Phys. Rev. B **89**, 195139 (2014).
[21] F. Dorfner, L. Vidmar, C. Brockt, E. Jeckelmann, and F. Heidrich-Meisner, Phys. Rev. B **91**, 104302 (2015).
[22] J. H. Fetherolf, D. Golež, and T. C. Berkelbach, Phys. Rev. X **10**, 021062 (2020).
[23] S. Engelsberg and J. R. Schrieffer, Phys. Rev. **131**, 993 (1963).
[24] J. Loos, M. Hohenadler, A. Alvermann, and H. Fehske, J. Phys.: Condens. Matter **18**, 7299 (2006).
[25] N. Prodanović and N. Vukmirović, Phys. Rev. B **99**, 104304 (2019).
[26] M. Berciu, Phys. Rev. Lett. **97**, 036402 (2006).
[27] B. Lau, M. Berciu, and G. A. Sawatzky, Phys. Rev. B **76**, 174305 (2007).
[28] M. Berciu and G. L. Goodvin, Phys. Rev. B **76**, 165109 (2007).
[29] G. L. Goodvin, M. Berciu, and G. A. Sawatzky, Phys. Rev. B **74**, 245104 (2006).
[30] G. L. Goodvin, A. S. Mishchenko, and M. Berciu, Phys. Rev. Lett. **107**, 076403 (2011).
[31] V. Janković and N. Vukmirović, Phys. Rev. B **105**, 054311 (2022).
[32] P. Mitrić, V. Janković, N. Vukmirović, and D. Tanasković, Phys. Rev. Lett. **129**, 096401 (2022).
[33] M. R. Carbone, D. R. Reichman, and J. Sous, Phys. Rev. B **104**, 035106 (2021).
[34] J. E. Hirsch, R. L. Sugar, D. J. Scalapino, and R. Blankenbecler, Phys. Rev. B **26**, 5033 (1982).
[35] H. De Raedt and A. Lagendijk, Phys. Rev. B **27**, 6097 (1983).
[36] N. V. Prokof'ev and B. V. Svistunov, Phys. Rev. Lett. **81**, 2514 (1998).
[37] A. S. Alexandrov and P. E. Kornilovitch, Phys. Rev. Lett. **82**, 807 (1999).
[38] V. Cataudella, G. De Filippis, A. S. Mishchenko, and N. Nagaosa, Phys. Rev. Lett. **99**, 226402 (2007).
[39] M. Hohenadler, H. G. Evertz, and W. von der Linden, Phys. Rev. B **69**, 024301 (2004).
[40] F. F. Assaad, Phys. Rev. B **78**, 155124 (2008).
[41] A. S. Mishchenko, N. Nagaosa, G. De Filippis, A. de Candia, and V. Cataudella, Phys. Rev. Lett. **114**, 146401 (2015).
[42] G. De Filippis, V. Cataudella, A. S. Mishchenko, N. Nagaosa, A. Fierro, and A. de Candia, Phys. Rev. Lett. **114**, 086601 (2015).
[43] E. Jeckelmann and S. R. White, Phys. Rev. B **57**, 6376 (1998).
[44] R. J. Bursill, R. H. McKenzie, and C. J. Hamer, Phys. Rev. Lett. **80**, 5607 (1998).
[45] C. Zhang, E. Jeckelmann, and S. R. White, Phys. Rev. B **60**, 14092 (1999).
[46] D. Jansen, J. Bonča, and F. Heidrich-Meisner, Phys. Rev. B **102**, 165155 (2020).
[47] S. Ciuchi, F. de Pasquale, S. Fratini, and D. Feinberg, Phys. Rev. B **56**, 4494 (1997).
[48] S. Fratini and S. Ciuchi, Phys. Rev. B **74**, 075101 (2006).
[49] H. De Raedt and A. Lagendijk, Phys. Rev. B **30**, 1671 (1984).
[50] D. J. J. Marchand and M. Berciu, Phys. Rev. B **88**, 060301(R) (2013).
[51] J. Bonča and S. A. Trugman, Phys. Rev. B **103**, 054304 (2021).
[52] Z. Li, C. J. Chandler, and F. Marsiglio, Phys. Rev. B **83**, 045104 (2011).
[53] C. J. Chandler and F. Marsiglio, Phys. Rev. B **90**, 245149 (2014).
[54] J. Bonča, S. A. Trugman, and M. Berciu, Phys. Rev. B **100**, 094307 (2019).
[55] B. Jusserand, D. Paquet, and F. Mollot, Phys. Rev. Lett. **63**, 2397 (1989).
[56] V. Y. Davydov, Y. E. Kitaev, I. N. Goncharuk, A. N. Smirnov, J. Graul, O. Semchinova, D. Uffmann, M. B. Smirnov, A. P. Mirgorodsky, and R. A. Evarestov, Phys. Rev. B **58**, 12899 (1998).
[57] The method that we use in principle can be expanded as well to two and even higher dimensions. It has been shown in Ref. [13] that, in the intermediate coupling regime, the method can yield ground state results for the energy in two and even three dimensions that are precise down to 10 significant digits in the thermodynamic limit. Due to the increasing complexity of the problem in higher dimensions when computing dynamic properties of the system, we have limited our calculations to 1D in this paper.
[58] C. Verdi, F. Caruso, and F. Giustino, Nat. Commun. **8**, 15769 (2017).
[59] F. Caruso, C. Verdi, S. Poncé, and F. Giustino, Phys. Rev. B **97**, 165113 (2018).
[60] C. Chen, J. Avila, S. Wang, Y. Wang, M. Mucha-Kruczyński, C. Shen, R. Yang, B. Nosarzewski, T. P. Devereaux, G. Zhang *et al.*, Nano Lett. **18**, 1082 (2018).

[61] Y. Wang, K. Nakatsukasa, L. Rademaker, T. Berlijn, and S. Johnston, Supercond. Sci. Technol. **29**, 054009 (2016).
[62] C. Cancellieri, A. S. Mishchenko, U. Aschauer, A. Filippetti, C. Faber, O. S. Barišić, V. A. Rogalev, T. Schmitt, N. Nagaosa, and V. N. Strocov, Nat. Commun. **7**, 10386 (2016).
[63] C. Lanczos, J. Res. Nat. Bur. Stand. **45**, 255 (1950).
[64] J. Jaklič and P. Prelovšek, Adv. Phys. **49**, 1 (2000).